Journal of Biomedical Optics

BiomedicalOptics.SPIEDigitalLibrary.org

Evaluation of silicon photomultipliers for multiphoton and laser scanning microscopy

Michael G. Giacomelli

SPIE.

Michael G. Giacomelli, "Evaluation of silicon photomultipliers for multiphoton and laser scanning microscopy," *J. Biomed. Opt.* **24**(10), 106503 (2019), doi: 10.1117/1.JBO.24.10.106503.

Journal of Biomedical Optics 24(10), 106503 (October 2019)

Evaluation of silicon photomultipliers for multiphoton and laser scanning microscopy

Michael G. Giacomelli*
University of Rochester, Department of Biomedical Engineering, Rochester, New York, United States

Abstract. The silicon photomultiplier (SIPM) is an emerging detector technology that enables both high sensitivity and high dynamic range detection of visible and near-infrared light at a fraction of the cost of conventional vacuum tube photomultiplier tubes (PMTs). A low-cost detection circuit is presented and the performance of a commercial SIPM is evaluated for high-speed laser scanning microscopy applications. For moderate-to-high-speed fluorescent imaging applications, the measurements and imaging results indicate that the SIPM exceeds the sensitivity of GaAsP PMTs, while providing higher dynamic range and better saturation behavior. For low speed or applications requiring large detector areas, the GaAsP PMT retains a sensitivity advantage due to large area and lower dark counts. The calculations presented show that, above a critical detection bandwidth, the SIPM sensitivity exceeds that of a GaAsP PMT.
[DOI: 10.1117/1.JBO.24.10.106503]

Keywords: multiphoton microscopy; fluorescence; silicon photomultiplier; surgical imaging.

Paper 190261R received Jul. 23, 2019; accepted for publication Sep. 24, 2019; published online Oct. 17, 2019.

1 Introduction

Photomultiplier tubes (PMTs), in which photoelectrons are multiplied through collisions with charged plates in a vacuum tube, emerged as the first practical means of detecting low light signals in the 1930s. Almost a century later, they remain in use in many areas of microscopy, medicine, and physics because of their exceptional combination of low noise, large bandwidth, and extremely high gain that enables efficient detection of signals as low as a single photon.[1] In particular, their unique combination of large detector area and large bandwidth enables them to collect diffuse signals in applications such as deep tissue imaging.[2] Unfortunately, compared to newer semiconductor sensors, PMTs have moderate quantum efficiency (QE), limited sensitivity in the infrared, are considerably more expensive to manufacture, have relatively large variation in single photon response, require very high voltage, and are much more easily damaged by excessive light exposure.

Recently, silicon photomultipliers (SIPMs) have emerged as a compelling and inexpensive method of detecting single photons in applications such as automotive LIDAR[3] where durability and cost are key constraints. In an SIPM, a parallel array of Geiger-mode avalanche photodiodes (APDs) is lithographically fabricated. When charged above their breakdown voltage, each APD acts as a photosensitive switch, transmitting a precise amount of stored charge in response to a single-photon excitation. While each APD acts in single-photon counting mode, the combination of thousands of detectors in parallel results in an effectively analog output. Although each APD requires a finite time to recharge between excitation events (typically tens of nanoseconds), the number of parallel diodes can be selected for the application such that photon pileup does not occur as in single-photon counting applications.[4] The combination of rapid recharging between excitations and large numbers of parallel diodes enables both single-photon sensitivity and linear dynamic range extending up to hundreds of billions of photons per second.[5]

Compared to conventional PMTs, SIPMs have advantages for biomedical microscopy applications that have not been widely explored. First, the use of silicon fabrication enables very low costs relative to vacuum tubes, low operating voltage, as well as extremely high damage thresholds. Furthermore, compared to photocathode materials, silicon diodes have high quantum efficiency in the near-infrared wavelengths used for deep tissue imaging.[6] Finally, the linearity at high power combined with high durability is an important advantage in many areas of medical imaging, where PMTs require specially designed overcurrent circuits and interlocks to avoid damage from normal clinic lights or from excessively bright samples. In contrast, SIPMs are routinely used for outdoor sensing applications and are exposed to direct sunlight.[3]

The resilience of SIPM detectors is particularly advantageous for imaging surgical pathology using techniques such as confocal fluorescence microscopy and two-photon microscopy. For example, in breast[7,8] prostate[9] and skin margin evaluation[10] surgical marking inks are applied directly to the margins of surgical excisions. Surgical inks are intensely fluorescent and are applied directly on top of the diagnostic regions of specimens. The intense fluorescence generated by surgical marking inks poses a challenge for PMTs, which can be overloaded or even damaged by exposure to intense light. Conversely, SIPMs saturate but do not overload and are not damaged by intense light.

In this work, I evaluate the use of an SIPM-based detector as compared to a high-sensitivity PMT for two-photon imaging. I specifically evaluate the use of each detector for imaging surgical pathology, but the results may be applicable to other applications of laser scanning microscopy. Compared to the PMT, I find that the SIPM has lower cost, covers a wider range of fluorophores, has lower excess noise, higher signal-to-noise ratio (SNR), and improved linearity at high signals. These attributes come at the expense of smaller detector area and higher

*Address all correspondence to Michael G. Giacomelli, E-mail: mgiacome@ur.rochester.edu

dark noise at ambient temperature. I show that for a number of operating conditions, especially those focusing on higher speed imaging, high dynamic range, or red-fluorescent samples, the SIPM offers superior performance.

2 Electrical Design and Characterization

For two-photon imaging, longer wavelength operation is generally preferred; thus, a red-enhanced (450 to 800 nm) S14420-3025 (Hamamatsu Photonics KK) was selected. This detector has a 3-mm circular diameter SIPM with a 25-μm APD pitch containing 11,344 parallel APDs and a peak sensitivity at 600 nm. 3 mm was selected because red-enhanced SIPMs have relatively high dark current (35 nA/mm^2 at 25°C) and because minimization of detector capacitance simplifies amplifier design at higher frequencies.

2.1 *Amplifier Design*

SIPMs are current output devices with a single-photon response that is a multiterm exponential decay. The two dominant terms in the response are the resistance–capacitance (RC) filter formed by the parallel capacitance of all APDs in the array with the external circuit's terminating resistance and the RC filter formed by the capacitance of an individual APD discharged through its internal quench resistor. The first term is common to all current output devices, including photodiodes and PMTs, and becomes a larger constraint as the overall active area increases. This can be addressed by either using a voltage amplifier with a suitable terminating resistance such that the RC filter bandwidth is set appropriately or using a transimpedance amplifier (TIA). This work uses a conventional TIA design with a 1500 Ω transimpedance gain. Combined with the 350pF capacitance of the S14420-3025 SIPM, this yields a 30-MHz bandwidth when used with a typical ~4 GHz gain-bandwidth op-amp, which was reduced to 24 MHz via post-filtering.

The second filter, formed by an individual APD's capacitance, is unique to SIPMs and scales with the size of individual avalanche diodes making up the array. As both gain and QE increase with increasing APD size, compensating for this effect electronically rather than choosing very small APD pixels is preferred. This work uses the pole-zero cancellation (PZC) method, which was developed previously.[11] Briefly, following the initial transimpedance amplification stage, an additional filter composed of a parallel resistor and capacitor is added such that the gain increases with frequency to cancel out the low-pass effect from the discharge time of each individual APD. In the time domain, this process can be thought of as keeping the sharp rising edge of the single-photon response (the high-pass signal passed by the capacitor) while canceling out the slow falling portion using current passed by the resistor. While this cancellation process attenuates ~80% to 90% of the total current emitted by the SIPM, it is applied after the TIA and thus attenuates both signal and electronic noise equally, resulting in a negligible effect on SNR. Finally, to compensate for the reduction in amplitude caused by the PZC circuit and the 50-ohm resistance needed to isolate the PZC capacitance from the TIA, a final voltage amplifier with a gain 12 was added, resulting in a total gain (seen from the TIA) of 6. The combined system functions as the series combination of a photodetector with a gain of 900,000 e-/pho, followed by a 1500-V/A transimpedance gain, then a PZC step that increases bandwidth by a factor of ~7, and finally a compensating gain stage (Fig. 1). The overall system response to a single-photon excitation is a ~10-ns pulse with an amplitude of 10 mV, although this value can be adjusted as needed for the analog to digital converter (A/D) voltage range.

The entire amplifier circuit (Fig 1, right frame) was integrated into a 1″-diameter circular printed circuit board (PCB) with the SIPM mounted opposite the TIA to minimize parasitic capacitance. Design files are available on https://github.com/mgiacomelli/sipm/. The amplifier/SIPM assembly was then mounted on an SM1 lens tube (Thorlabs, Inc.) and screwed into the collection optics of a commercial two-photon scope (Bergamo-2, Thorlabs). SIPM bias was provided by a commercial charge pump DC–DC converter (HV80B, AIT Instruments). Figure 2 shows the assembled detector and amplifier transfer function. Additional collection optics were aligned in the lens tube to adapt the expected 5-mm PMT diameter of the microscope to the 3-mm diameter of the SIPM detector. Zemax simulations of the beam path indicated that all light passed from a 20-mm back aperture over $+/-3$ deg was successfully relayed onto the 3-mm detector. For a 10× objective, this corresponds to a negligible vignette over a 2.1-mm field of view at 0.45 numerical aperture and a gradual loss of collection efficiency for photons emitted at larger field angles.

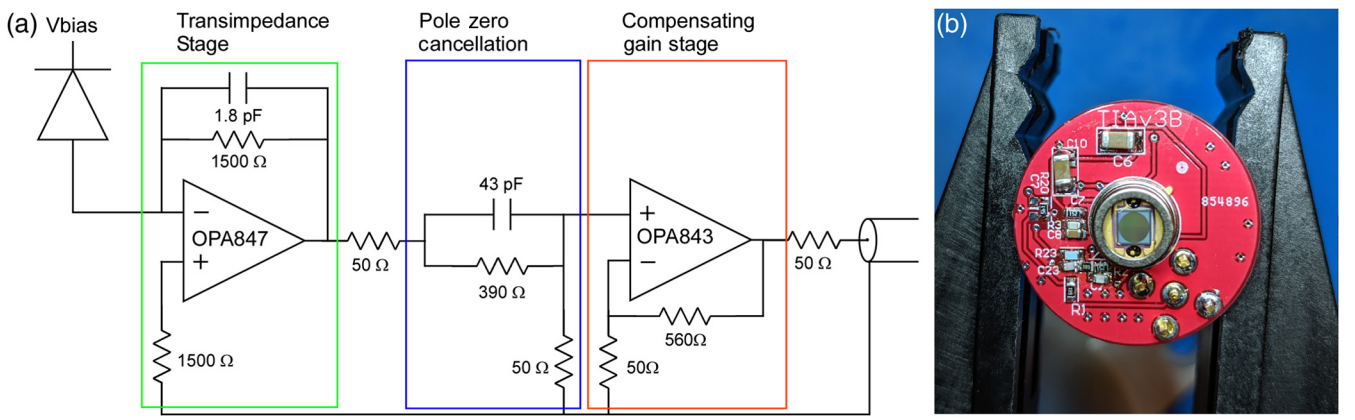

Fig. 1 SIPM detector module: (a) circuit diagram and (b) assembled circuit. The SIPM was integrated into a PCB incorporating a transimpedance gain stage with a gain of 1500 ohms (green box), a PZC circuit to shape the detector output (blue box), and an additional gain stage (red box) that compensates for the gain lost during the previous pulse-shaping stage.

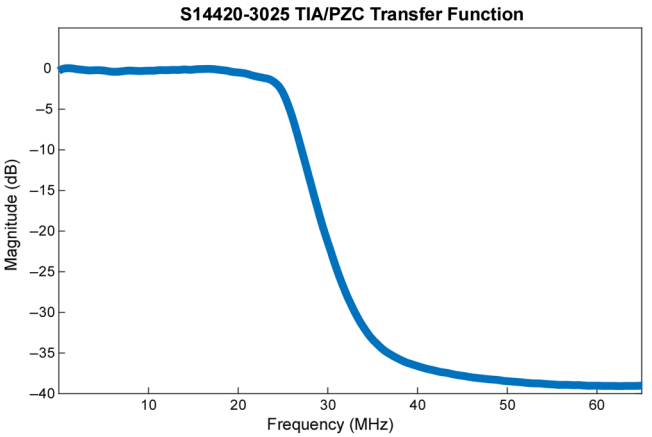

Fig. 2 Measured SIPM, amplifier, and PZC transfer function with 24-MHz low-pass filter.

2.2 *Photomultiplier Tube Selection*

The Thorlabs PMT2100, a combination of a USB-powered low-noise 80-MHz TIA and a Hamamatsu H10770-40P PMT module mounted on a shielded enclosure, was selected. The H10770-40 is among the most widely used photomultipliers for two-photon imaging and is distributed in the common H7422-40 module from Hamamatsu as well as in commercial multiphoton microscopes. The H10770-40 uses a GaAsP photocathode with a >40% peak QE, while the "P" model is an H10770 with the lowest dark noise and highest QE in a production run. The H10770-50 is also available with a GaAs photocathode with an extended range above 700 nm but with much lower absolute quantum efficiency.[12] The tested H10770-40P has a specified 51% photocathode QE at peak wavelength (~550 nm) and an effective photon detection efficiency (PDE) of 40% to 45% after (gain-dependent) dynode losses. The properties of both detectors are summarized in Table 1.

Table 1 Detector properties.

	H10770-40PA	S14420-3025
Gain range (e-/pho)	50,000 to 5×10^6	500,000 to 1,700,000
Nominal gain (e-/pho)	100,000	1×10^6 (150,000 after PZC)
Peak PDE at nominal gain	40%, 550 nm	30%, 590 nm
ENF	~1.35	~1.04
Noise-equivalent QE (PDE/ENF)	0.29	0.28
Measured dark count @ 25C (s^{-1})	2500	1,600,000
Active area	5-mm diameter	3-mm diameter
Maximum counts per second at nominal gain	3×10^9	100×10^9

3 Results

3.1 *Signal-to-Noise Ratio*

To evaluate the relative performance of the S14420-3025 SIPM, a 50:50 beamsplitter (BSW10R, Thorlabs) plate was used to evenly distribute light from fluorescent samples between SIPM and GaAsP PMT. A uniform fluorescent slide with emission peak at 570 nm (FSK4, Thorlabs; selected because its emission aligns with the region of overlap between the peak sensitivity of both detectors) was used to acquire sets of 10 uniform frames at 32 MP/s over 1 mm^2 (effective analog bandwidth of 7.9 MHz) at increasing power levels. Both detectors were configured with identical 24-MHz low-pass filters. The per-pixel variance and mean values were used to calculate the number of detected photons striking the SIPM using the photon transfer curve[13] (PTC) method. Briefly, the PTC method computes the gain of a detector (in A/D levels per photon), using the equality of the mean and variance of shot noise. While the PTC method cannot be directly used for detectors such as PMTs that have excess noise factor (ENF) $\gg 1$ because both photon shot noise and excess noise contribute to variance, the negligible ENF (1.04 at 47 V) of the SIPM enables computing its gain using the PTC method. Once the gain of the SIPM is known, the number of photons striking each detector can be calculated from the specified QE, and SNR determined as a function of photon flux.

Plots of SNR versus incident photons for both detectors are presented in Fig. 3. For the H10770 PMT, SNR is only weakly affected by control voltage (Fig. 3, top), while gain is exponential in voltage. At a control voltage of ~0.55 v, the PMT exceeds the gain of the SIPM and more rapidly saturates at higher gains. Consequently, the maximum achievable SNR occurs at the lowest gain voltage. Conversely, the SIPM gain only increases linearly with voltage, while the SNR is much more strongly affected by control voltage (Fig. 3, bottom). At the recommended control voltage of 47 v, the S14420-3025 SNR is nearly identical to the H10770-40PA. Surprisingly, SNR continues to improve with increasing control voltages beyond maximum datasheet value (49 v), and improves a further 5% from 49 to 51 v where it has an 11.9% advantage over the H10770 at 0.5 v.

3.2 *Tissue Imaging*

Discarded tissue specimens not required for diagnosis were acquired from the University of Rochester Medical Center under a protocol approved by the Research Subjects Review Board (Study 3085). A selected skin specimen was stained with acridine orange (AO, emission wavelength equal to peak GaAsP sensitivity) and then imaged using the 50:50 beam splitter to enable both detectors to each simultaneously detect half of the emitted light while configured at 47 v (SIPM) and 0.5 v (PMT). As errors in setting the zero point for either image could bias the results, a 14-bit A/D was used to record $+/-1$ V, and the zero point was estimated as the mean of a dark frame minus one standard deviation of the same frame. This ensures that a minimum number of pixels are clipped to zero by electronic noise. Finally, both images were histogram normalized such that the gain in each image was equal. Results are presented in Fig. 4, where both channels are visually identical as predicted from the PTC, while Fig. 5 shows a histogram of pixel values after histogram equalization.

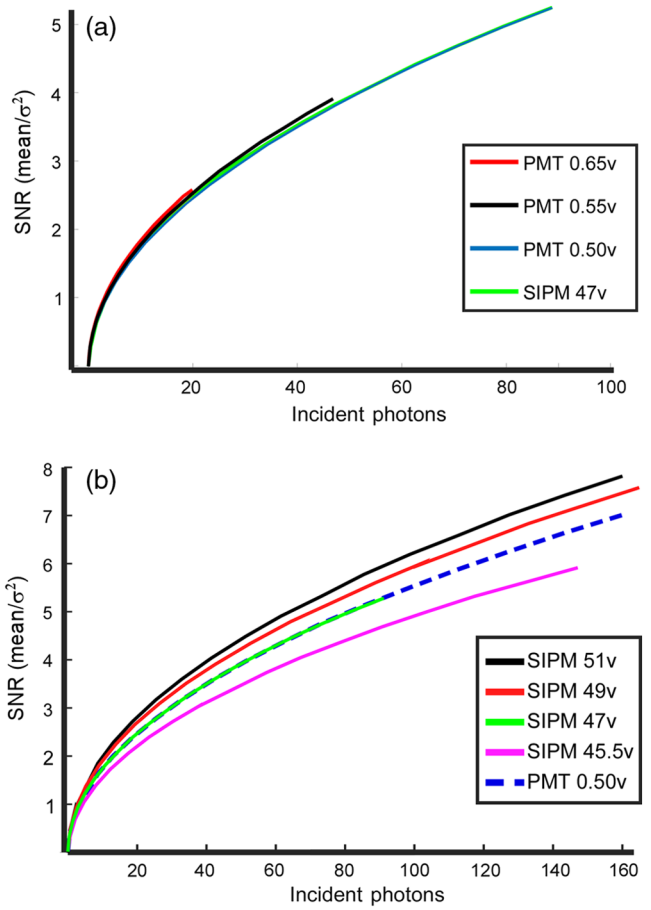

Fig. 3 SNR versus incident power computed for the S14420-3025 SIPM and H10770-40PA PMT. All curves show shot-noise-limited statistics with the SNR (defined as mean divided by standard deviation) equaling the square root of the mean photoelectrons. The number of photons incident is calculated using the specified PDE (29%) and ENF (1.04) of the SIPM at 47v via the PTC method. (a) The PMT shows a small increase in SNR with increasing control voltage, but saturation causes the maximum possible SNR to decrease with increasing gain. (b) In contrast, the SIPM SNR increases much more rapidly with increasing voltage and continues to increase up to the maximum tested voltage. Note that the SIPM at 47v (green line) is duplicated in both plots. Above 47v, the SIPM exceeds the SNR of the GaAsP PMT.

3.3 *Dynamic Range and Saturation*

To test the saturation behavior of both detectors, the beam splitter was replaced with a dichroic filter and fluorescently labeled a skin cancer specimen with the DNA label AO (PMT channel) and the protein label SR101 (SIPM channel). Video-rate frames were recorded while the specimen was examined in real time, simulating a workflow where a surgical margin was evaluated for the presence of cancer. Frames were then stitched into a mosaic using a method described previously[8] and rendered as virtual hematoxylin and eosin slides.[15] Imaging a localized bright region with infiltrative basal cell carcinoma resulted in saturation of both detectors (Fig. 6). This triggered the overcurrent protection on the PMT. In contrast, some SIPM pixels are saturated, but imaging is otherwise unaffected, demonstrating the higher dynamic range and durability of the SIPM.

4 Discussion

I present a simple, extremely low-cost photodetector module based on a red-enhanced silicon photomultiplier. I combined the detector with a TIA circuit and a PZC filter, which enabled a flat amplifier bandwidth >24 MHz, although this could be adjusted over a wider range. To facilitate integration into existing microscopes, the entire detector and amplifier module was assembled onto a 1-in. PCB that could be mounted on a standard SM1 lens tube. This amplifier configuration was relatively simple, required only a few dollars' worth of components, and was sufficient to provide a noise floor significantly below that of the detector.

Compared to the dark count rate of the H10770-40P, the S14420-3025 has dramatically higher dark count rates (>600 times), which might be expected to negatively impact the dynamic range of the SIPM. However, the SNR of a detector with photoelectron gain is limited by the sum of both signal and dark shot noise:[16]

$$\mathrm{SNR} = \frac{I_s}{\sqrt{2 \times q \times F \times B \times G \times (I_s + I_d)}}, \tag{1}$$

where I_s is the signal current, q is the charge of an electron, F is the ENF, B is the detection bandwidth, G is the detector gain, and I_d is the dark current. The signal current can be further expressed as

$$I_s = \frac{P \times \mathrm{PDE} \times G \times q}{\mathrm{PE}}, \tag{2}$$

where P is the optical power and PE is the photon energy in joules. For I_s much more than I_d, the effect of dark noise on total SNR is small, relative to photon shot noise. Recognizing that I_s is proportional to the number of photons detected per pixel, the SNR can be increased by either making the signal more intense or increasing the dwell time per pixel. By setting $\mathrm{SNR} = 1/\sqrt{2}$ and solving for bandwidth that gives $I_s = I_d$, the bandwidth where dark current shot noise first exceeds the minimum optical shot noise can be calculated as

$$\mathrm{BW}_{\mathrm{dark}} = \frac{I_d}{2 \times q \times F \times G}. \tag{3}$$

Neglecting the ENF F, which is close to unity for the S14420-3025, $\mathrm{BW}_{\mathrm{dark}}$ is 780 KHz. Intuitively, this is the detection bandwidth that gives approximately one dark count per resolvable point; thus, at higher bandwidths, optical shot noise dominates. For lower bandwidths, dark counts become numerous enough to begin to obscure signal in pixels with lower photon counts. Thus, for typical resonant scanning bandwidths (5 to 25 MHz), the dark shot noise contributions from both the SIPM and the PMT are negligible, and dark current has no effect on SNR. This result is illustrated in Fig. 4, where at a 7.9-MHz signal bandwidth, the nearly 3 order of magnitude reduction in dark noise for the PMT has no discernable effect on the total noise.

Conversely, when used with galvanometer scanning (bandwidth typically between 0.1 and 0.5 MHz), the dark shot noise of the red-enhanced SIPM at room temperature becomes sufficient to overcome signal shot noise in darker pixels, negatively impacting overall dynamic range. In this operating regime, either a lower dark count detector or subambient cooling is

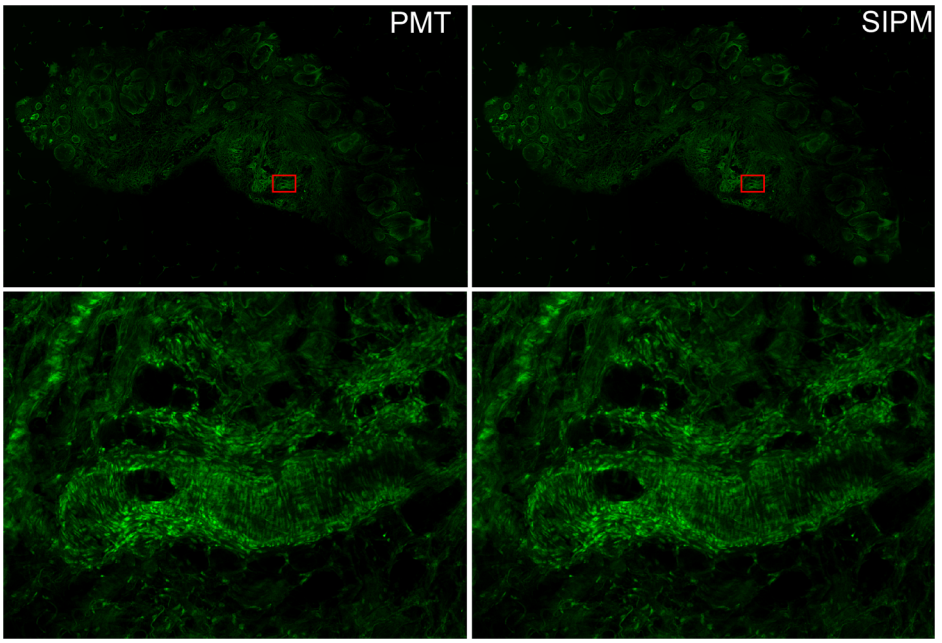

Fig. 4 Human skin specimen labeled with AO and imaged using the H10770-40PA (labeled PMT) and the S14420-3025MG (labeled SIPM) using a 50:50 beam splitter. Power levels were set to the maximum permissible for the PMT without triggering the overcurrent behavior. Examination of the region with both intense fluorescent signal and nonfluorescent regions reveals minimal difference. For full resolution dataset, see Ref. 14.

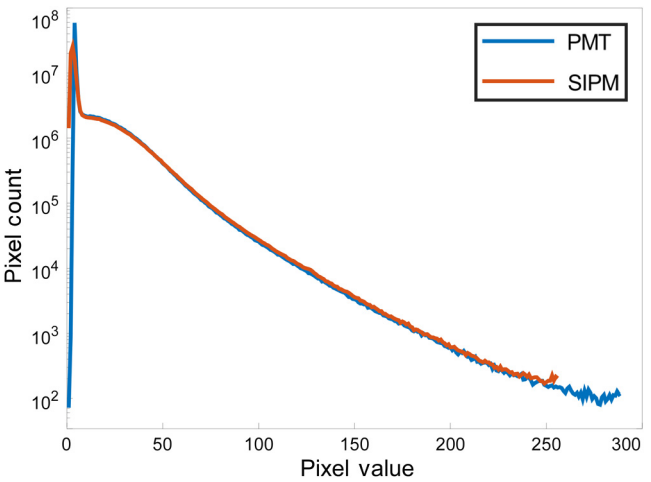

Fig. 5 Histogram of pixel values taken from Fig. 4 prior to image stitching and vignette correction but after histogram normalization. For clarity, values were not clamped at 255 and a DC offset of 2 pixel levels was added.

needed to preserve full dynamic range. For example, the lower noise S13360 (Hamamatsu, $BW_{dark} = 250$ KHz) or the thermoelectric (TEC)-cooled S13362 (Hamamatsu, $BW_{dark} = 12.5$ KHz) will retain the dynamic range of the S14420 when lower speed galvanometer scanning is used, although SNR was not evaluated for these detectors. While subambient cooling is more costly than ambient temperature operation, it is still likely to be substantially cheaper than a GaAsP or GaAs PMT for an equivalent dark count rate, although at very low detection bandwidths, when very large active areas are required or when photon counting, the H10770-40P ($BW_{dark} < 2$ KHz) retains an advantage due to its incredibly low dark shot noise and larger active area. Although no GaAs PMT was available to evaluate, the much lower specified QE values suggest that the SIPM advantage should be significantly larger than was observed for the GaAsP PMT. Furthermore, it is important to note that the simple amplifier design here would begin to limit dynamic range when paired with a lower dark count detector and lower detection bandwidths, necessitating the use of a more sophisticated design.

The comparable or superior SNR curves for the SIPM are initially surprising, given the ~50% higher nominal photocathode QE of the PMT, which would be expected to give a substantial reduction in shot noise and thus higher SNR. However, the nominal photocathode QE does not directly translate into improved shot noise limited performance because, especially at lower gains (Fig. 3), not all photoelectrons are successfully amplified by the dynode chain,[17] resulting in a somewhat lower PDE. Furthermore, in a detector with gain noise, the shot noise-limited SNR calculated from the PDE is divided by the ENF, resulting in a noise variance equal to that of a detector with a lower PDE but without gain noise. In the case of the H10770-40P, no ENF is specified, but measurement of the pulse height spectrum for this specific PMT yielded mean gain value of 2.9 times the gain variance that was relatively independent of control voltage, or an F (excluding afterpulsing, which is negligible at low gain) of ~1.35, similar to the values reported previously for the same model.[17] The excess noise of the S14420-3025 is 1.04 at the nominal gain. Using these values, I define a shot-noise-equivalent QE equal to PDE/F (Table 1) that gives the quantum efficiency of a detector with no gain noise that would appear to have the same shot noise-limited SNR. According to this measure, the H10770-40PA should have nearly equal SNR to the S14420 at low gain, in good agreement with measurements using the PTC. At higher gains, the PDE/F of the SIPM increases much faster than the PMT, resulting in

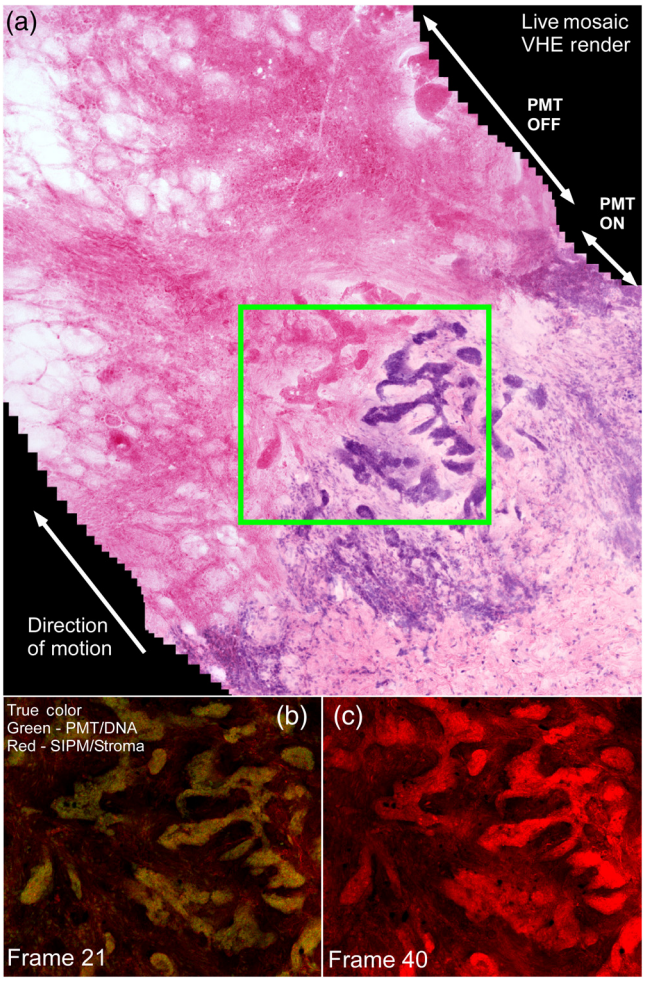

Fig. 6 Overcurrent behavior of both detectors demonstrated in a mosaic stitched from individual video frames acquired from a skin cancer specimen. (a) On frame 22, a region of intense basal cell carcinoma saturates both detectors, resulting in the PMT overcurrent protection circuit activating to avoid damage. In contrast, the SIPM is not damaged by intense light and, while individual pixels saturate, the detector continues to function normally. (b) Frame 21 shows the signal just before saturation without VHE rendering, while (c) frame 40 shows both detectors fully saturated and the PMT disabled by overcurrent.

better SNR with increasing gain. Furthermore, because the SIPM does not saturate at reasonable light levels, there is no loss of dynamic range from higher gain as there is with the PMT. Therefore, for high-speed scanning applications, an SIPM with low excess noise operated at very high gain maximizes both SNR and dynamic range.

While the GaAsP PMT retains a small PDE advantage, the excess noise of SIPM detectors has improved rapidly in recent years,[6] resulting in overall better SNR than a GaAsP PMT when used at detection bandwidths where the effect of dark current is negligible. It is interesting to note that the PDE of the S14420-3025 is limited by the relatively low fill factor (63%) of the APDs because the quench resistors are mounted on top of the detector and therefore block a large fraction of incident photons. A hypothetical back-illuminated SIPM or front-illuminated SIPM with microlens array with the same per-area sensitivity but a higher fill factor could have significantly higher noise-equivalent QE.

5 Conclusion

I have demonstrated a low-cost solution for high-sensitivity detection in laser scanning microscopy based on a low-cost TIA and SIPM detector. In applications such as high-speed two-photon microscopy, rapid improvements in SIPM detectors now enable better sensitivity to GaAsP PMTs at much lower cost, while covering a wider range of wavelengths, dynamic range, and saturation behavior. SIPMs have further advantages in durability and are not damaged by intense light, making them more suitable for some biomedical applications, such as clinical imaging, where intense light may be present. For lower speed imaging, using low-speed galvanometers, either PMTs or SIPMs, may be preferred depending on the detection bandwidth and if TEC cooling is available. In all cases, selection of detectors with the appropriate dark count rate for the detection bandwidth is critical.

Disclosures

The author has no conflict of interest to disclose.

Acknowledgments

I thank Bill Radtke for his insightful comments on amplifier design and assistance with circuit modeling. I also thank Dr. Sherrif Ibrahim for providing tissue specimens. Finally, I thank Dino Butron and Kathryn Pritchard of Hamamatsu for their insight on detector characterization. This study was supported by the U.S. National Institutes of Health, Grant No. K22-CA226035-01.

References

1. Hamamatsu, *Photomultiplier Tubes, Basics and Applications*, 3rd ed., pp. 45–46, Hamamatsu Photonics, Japan (2007).
2. J. P. Zinter and M. J. Levene, "Maximizing fluorescence collection efficiency in multiphoton microscopy," *Opt. Express* **19**(16), 15348 (2011).
3. R. Agishev et al., "LIDAR with SiPM: Some capabilities and limitations in real environment," *Opt. Laser Technol.* **49**(July), 86–90 (2013).
4. P. Eraerds et al., "SiPM for fast photon-counting and multiphoton detection," *Opt. Express* **15**(22), 14539 (2007).
5. SensL Corporation, "Introduction to SiPM—technical note," 2017, https://www.sensl.com/downloads/ds/TN%20-%20Intro%20to%20SPM%20Tech.pdf.
6. F. Acerbi et al., "Silicon photomultipliers: technology optimizations for ultraviolet, visible and near-infrared range," *Instruments* **3**(1), 15 (2019).
7. T. Yoshitake et al., "Direct comparison between confocal and multiphoton microscopy for rapid histopathological evaluation of unfixed human breast tissue," *J. Biomed. Opt.* **21**(12), 126021 (2016).
8. M. G. Giacomelli et al., "Multiscale nonlinear microscopy and wide-field white light imaging enables rapid histological imaging of surgical specimen margins," *Biomed. Opt. Express* **9**(5), 2457 (2018).
9. L. C. Cahill et al., "Comparing histologic evaluation of prostate tissue using nonlinear microscopy and paraffin H&E: a pilot study," *Mod. Pathol.* **32**(8), 1158–1167 (2019).
10. M. G. Giacomelli et al., "Comparison of nonlinear microscopy and frozen section histology for imaging of Mohs surgical margins," *Biomed. Opt. Express* **10**(8), 4249 (2019).
11. A. Gola, C. Piemonte, and A. Tarolli, "Analog circuit for timing measurements with large area SiPMs coupled to LYSO crystals," *IEEE Trans. Nucl. Sci.* **60**(2), 1296–1302 (2013).
12. Y. Wang et al., "Comparison of signal detection of GaAsP and GaAs PMTs for multiphoton microscopy at the 1700-nm window," *IEEE Photonics J.* **8**(3), 1–6 (2016).
13. M. J. DeWeert et al., "Photon transfer methods and results for electron multiplication CCDs," *Proc. SPIE* **5558**, 248–259 (2004).
14. M. G. Giacomelli, Figure 4, https://imstore.circ.rochester.edu/papers/sipm/Fig4.html (2019).

15. M. G. Giacomelli et al., "Virtual hematoxylin and eosin transillumination microscopy using epi-fluorescence imaging," *PLoS One* **11**(8), e0159337 (2016).
16. G. Adamo et al., "Silicon photomultipliers signal-to-noise ratio in the continuous wave regime," *IEEE J. Sel. Top. Quantum Electron.* **20**(6), 284–290 (2014).
17. J. Pawley, *Handbook of Biological Confocal Microscopy*, pp. 77–78, Springer Science & Business Media, Boston, Massachusetts (2010).

Michael G. Giacomelli is an assistant professor at the University of Rochester, New York. He received his MS degree in electrical engineering and his PhD in biomedical engineering from Duke University in 2012. He is the author of more than 25 journal papers and has written two book chapters. His current research interests include multiphoton microscopy, digital histology, and surgical imaging. He is a member of SPIE.